Mapping the Design Space of a Recuperated, Recompression, Precompression Supercritical Carbon Dioxide Power Cycle with Intercooling, Improved Regeneration, and Reheat

Andy Schroder* Mark Turner†
University of Cincinnati, Cincinnati, OH, 45221, U.S.A.

Abstract

A real fluid heat engine power cycle analysis code has been developed for analyzing the zero dimensional performance of a recuperated, recompression, precompression supercritical carbon dioxide power cycle with intercooling, improved regeneration, and reheat. Variation in fluid properties within the heat exchangers is taken into account by discretizing zero dimensional heat exchangers. Variation in performance with respect to design heat exchanger pressure drops, precompressor pressure ratio, main compressor pressure ratio, recompression mass fraction, main compressor inlet pressure, and low temperature recuperator mass fraction have been explored throughout a range of each design parameter. Real turbomachinery efficiencies are implemented and the sensitivity of the cycle performance and the optimal design parameters is explored. Sensitivity of the cycle performance and optimal design parameters is also studied with respect to the minimum heat rejection temperature and the maximum heat addition temperature. An interactive web based tool has been developed for analyzing the performance of the entire design space in greater detail as well as plotting temperature difference within the heat exchangers.

Nomenclature

ΔT	temperature difference between a heat exchanger's cooled and heated sides ($T_{Cooled} - T_{Heated}$), K
$\dot{m}_{Cooled}$	mass flow rate of a heat exchanger's cooled fluid, kg/s
$\dot{m}_{Heated}$	mass flow rate of a heat exchanger's heated fluid, kg/s
η	turbomachine isentropic efficiency
ϕ	fraction of desired heat transferred
c_p	specific heat at constant pressure, $J/(kg*K)$
C_{Cooled}	specific heat at constant pressure of a heat exchanger's cooled fluid, based on the mass flow rate of the heat exchanger's cooled fluid, $J/(kg*K)$
C_{Heated}	specific heat at constant pressure of a heat exchanger's heated fluid, based on the mass flow rate of the heat exchanger's cooled fluid, $J/(kg*K)$
$c_{p,Cooled}$	specific heat at constant pressure of a heat exchanger's cooled fluid, $J/(kg*K)$
$c_{p,Heated}$	specific heat at constant pressure of a heat exchanger's heated fluid, $J/(kg*K)$
d	heat exchanger pressure drop coefficient, Pa/K
h	total enthalpy, J/kg
$h_{i,Cooled}$	total enthalpy of a heat exchanger's cooled fluid, at the heat exchanger cooled side inlet, J/kg
$h_{i,Heated}$	total enthalpy of a heat exchanger's heated fluid, at the heat exchanger heated side inlet, J/kg
h_i	total enthalpy at a turbomachine inlet, J/kg
$h_{o,Cooled}$	total enthalpy of a heat exchanger's cooled fluid, at the heat exchanger cooled side outlet, J/kg
$h_{o,Heated}$	total enthalpy of a heat exchanger's heated fluid, at the heat exchanger heated side outlet, J/kg
$h_{o,max,Heated}$	maximum possible total enthalpy of a heat exchanger's heated fluid, at the heat exchanger heated side outlet, J/kg
$h_{o,min,Cooled}$	minimum possible total enthalpy of a heat exchanger's cooled fluid, at the heat

*Graduate Student, Corresponding Author, Email: info@AndySchroder.com
†Associate Professor of Aerospace Engineering

	exchanger cooled side outlet, J/kg
h_o	total enthalpy at a turbomachine outlet, J/kg
$h_{p,Cooled}$	total enthalpy of a heat exchanger's cooled fluid, at the heat exchanger pinch point, J/kg
$h_{p,Heated}$	total enthalpy of a heat exchanger's heated fluid, at the heat exchanger pinch point, J/kg
p	total pressure, Pa
p_i	turbomachine inlet total pressure, Pa
p_o	turbomachine outlet total pressure, Pa
$p_{i,Cooled}$	total pressure of a heat exchanger's cooled fluid, at the heat exchanger cooled side inlet, Pa
$p_{i,Heated}$	total pressure of a heat exchanger's heated fluid, at the heat exchanger heated side inlet, Pa
$p_{p,Cooled}$	total pressure of a heat exchanger's cooled fluid, at the heat exchanger pinch point, Pa
$p_{p,Heated}$	total pressure of a heat exchanger's heated fluid, at the heat exchanger pinch point, Pa
PR_c	compressor pressure ratio, p_o/p_i
PR_t	turbine pressure ratio, p_i/p_o
s	entropy, J/kg
s_i	turbomachine inlet entropy, J/kg
T	total temperature, K
T_i	turbomachine inlet total temperature, K
T_o	turbomachine outlet total temperature, K
T_p	heat exchanger pinch temperature, K
T_{Cooled}	heat exchanger cooled side temperature, K
T_{Heated}	heat exchanger heated side temperature, K
$T_{i,Cooled}$	total temperature of a heat exchanger's cooled fluid, at the heat exchanger cooled side inlet, K
$T_{i,Heated}$	total temperature of a heat exchanger's heated fluid, at the heat exchanger heated side inlet, K
$T_{o,Cooled}$	total temperature of a heat exchanger's cooled fluid, at the heat exchanger cooled side outlet, K
$T_{o,Heated}$	total temperature of a heat exchanger's heated fluid, at the heat exchanger heated side outlet, K
W	turbine work, J/kg

1 Introduction

Closed loop Brayton cycles utilizing Supercritical CO_2 (S-CO_2) as their working fluid have gained interest in recent years for electrical power generation due to potentially high real cycle thermal efficiencies. The high efficiencies of closed loop Supercritical CO_2 Brayton cycles may be possible because operation with the compression phase near the critical point results in a cycle that possesses favorable qualities of both the closed loop water Rankine Cycle and the traditional open loop air Brayton Cycle. Design of such cycles requires complex analysis to consider completely real fluid property variations, which are a function of both temperature and pressure.

The S-CO_2 Brayton cycle features low compression work (low back work ratio) when compared to a traditional open loop air Brayton cycle. The lower back work ratio results in a decreased sensitivity of compressor isentropic efficiency (and the isentropic efficiency of the turbine that drives the compressor) on the cycle efficiency. Non-condensing cycles have a narrow heat addition and heat rejection temperatures that does not require evaporative cooling, but still approximates a Carnot cycle better than an open loop Brayton cycle. Because the S-CO_2 Brayton cycle does not have to reject latent heat of vaporization at a constant temperature, more recuperation is possible and the cycle is more appropriate for dry cooling in hot climates than traditional closed loop water Rankine cycles because more of the heat can be rejected at higher temperatures. Proposed S-CO_2 cycles are typically recuperated cycles which also results in a much lower pressure ratio than an unrecuperated cycle. Unrecuperated cycles need higher pressure ratios in order to be efficient because if the pressure ratio is too low, too much energy will not be extracted by the turbine(s) and will be wasted. Recuperated cycles can have lower pressure ratios because they are able to recover energy that is not extracted by the turbine(s) and transfer it back to the high pressure side of the cycle. CO_2 is a gas of choice because it is cheap, inert, non-toxic, and its critical temperature of 304K (31°C) is near ambient temperature, ∼294K (21°C). In addition, the S-CO_2 Brayton cycle features very high power densities due to the high fluid density that occurs because of the high pressures throughout the cycle and the high molecular weight of CO_2 when compared to water or air.

Possible applications for S-CO_2 engines include base load terrestrial electrical power generation, marine, aviation, and spacecraft electrical power generation. A S-CO_2 engine could be configured as a bottom-

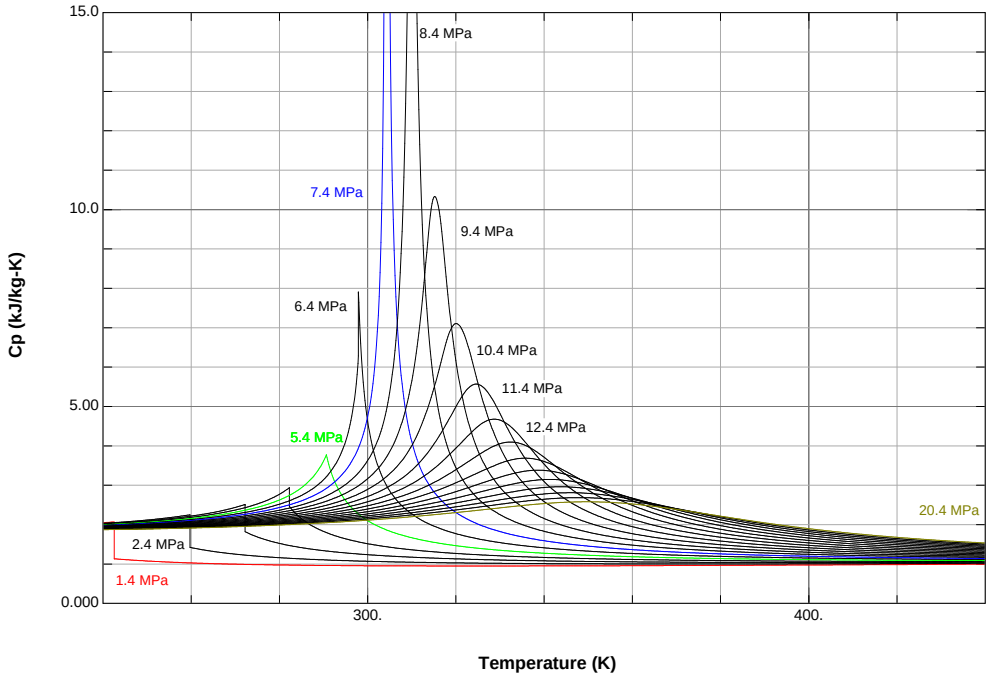

Figure 1: Specific Heat (c_p) vs Temperature at various Pressures for Carbon Dioxide. The blue line indicates the critical pressure of 7.4MPa.

ing cycle using waste heat from a traditional open loop gas turbine (traditional Brayton cycle) or as a primary cycle with nuclear and solar energy heat sources. It's also possible that a S-CO_2 could serve as a primary cycle with the combustion of fossil fuels such as coal and natural gas as a heat source, although the benefit in this configuration has not yet been explored in depth.

Although there are many potential advantages of S-CO_2 Brayton cycles, design, development, and testing of the appropriate turbomachinery proves to be a very challenging task. The critical pressure of carbon dioxide is 7.4 MPa. The high pressures required for operation near the critical point results in increased structural loading of components, as well as very high working fluid densities. High working fluid densities result in significantly smaller turbomachinery that must be operated at higher speeds than most familiar turbomachinery and prohibit efficient low power, low speed, low cost prototypes to be developed. These high speed requirements inhibit ease of testing of small turbomachinery and small S-CO_2 Brayton cycles. Strong property gradients near the critical point present additional design challenges due to the variation in fluid properties within the turbomachinery components. Figure 1 illustrates the non-linearity of the specific heat of carbon dioxide near the critical point at different temperatures and pressures. Figure 1 was created using REFPROP's Graphical User Interface [1]. Off design operation subjects the turbomachinery to very different inlet conditions. This presents an additional difficulty in developing appropriate technologies that can operate efficiently and stall free throughout a wider operating range and utilize the lower heat rejection temperatures possible with variations in ambient air temperature with time of day, season, and geographic location. These lower heat rejection temperatures could result in a higher cycle efficiency. These challenges are particularly strong in the main compressor which operates near, or at the critical point of CO_2.

The high pressures also present increased structural loading and seal leakage issues, which are even more challenging due to the high operating speeds. Nonlinear specific heat mismatch between the high and low pressure sides of the cycle causes limitations exchanging heat between high and low pressure sides, particularly at lower temperatures and increased complexity in modeling and optimizing the cycle layout. The closed loop design presents additional system complexities.

Because of all of these design challenges, it is important to establish a well directed development process in order to have a successful and efficient maturity of the components and system. This work investigates the impact of system layout, component efficiency, and operating conditions on sizing of the components in the system and the overall system efficiency. Due to the highly variable fluid properties the sensitivity

of component efficiencies will change at different operating conditions. As a result, as cycle layout and component sizes change, the sensitivity of the component efficiencies will also change. Understanding these relationships is important during design and testing because it helps impact the overall direction of the development process. For example, a development engine's layout, components, and overall performance may be radically different from what is targeted for a production engine. One may choose to design an engine with a lower overall performance in order focus on the design and testing of a particular component that could be installed in a completely different size production engine. One may also design and build components of lower efficiency and different performance than a production engine, just to test an overall cycle layout.

2 Prior Work

The earliest reference to a supercritical carbon dioxide power cycle is that of a patent by Sulzer in 1948[2]. Among other efforts within the 1900s, studies conducted by Angelino[3, 4] and Feher[5] in the 1960s were significant contributes to the field. Vaclav Dostal revived interest in supercritical carbon dioxide power cycles with the publication of his doctoral dissertation in 2004[6]. Dostal reviewed and compared a number of cycles and layouts, and primarily analyzed a simple recuperated S-CO_2 cycle with reheat and intercooling and a simple recompression S-CO_2 cycle in his dissertation. He explored heat exchanger volumes and pressure drops in the simple and recompression cycles. Dostal researched application specifics, economic analysis, plant layouts, and control schemes for use of the recompression cycle with nuclear reactors.

Sandia National Laboratories has developed two supercritical CO_2 test rigs with their contractor, Barber-Nichols. Their efforts were initially motivated by nuclear power applications. Sandia's two test rigs have included both a simple S-CO_2 cycle and a recompression S-CO_2 cycle. They have successfully achieved startup of both a main compressor/turbine and recompressor/-turbine loop. Their rigs have incorporated turbine alternator/generator compressor assemblies which has limited their operating speeds to that of the maximum speed of the alternator/generator[7, 8]. Bechtel Marine Propulsion Corporation has also been constructing and operating a similar test rig to that of Sandia's[9].

Echogen Power Systems has been developing an engine for waste heat recovery applications since 2007[10]. The United States Department of Energy began subsidizing the development of engines for concentrating solar power applications in mid 2012[11, 12, 13].

3 Methodology

3.1 Cycle Layout

The layout for the most general cycle considered is shown in Figures 2-5 and a summary of the state points is shown in Table 1. Figure 2 shows the thermodynamic states on a Temperature Entropy diagram ($T-s$) for an example cycle configuration. The contours in Figure 2 are colored by the specific heat of the fluid of all states within a certain range. Black lines indicate the thermodynamic states throughout the cycle and the numbered points indicate key component inlet and outlet states. Colored lines indicate constant pressure lines starting at each of these numbered state points, and the corresponding pressures are indicated in the legend. Because of the low pressure drop within many components, it is difficult to distinguish the difference in many of these constant pressure lines without magnifying the figure dramatically. Figure 3 is similar to 2, except the horizontal axis is pressure. The fluid type for each region is also labeled. The liquid vapor dome is collapsed to a single line in Temperature Pressure ($T-p$) diagrams. Figure 4 is a schematic which shows the main component types in the proposed system, which include heat exchangers, turbomachines, shafts, tanks, piping, and a generator.

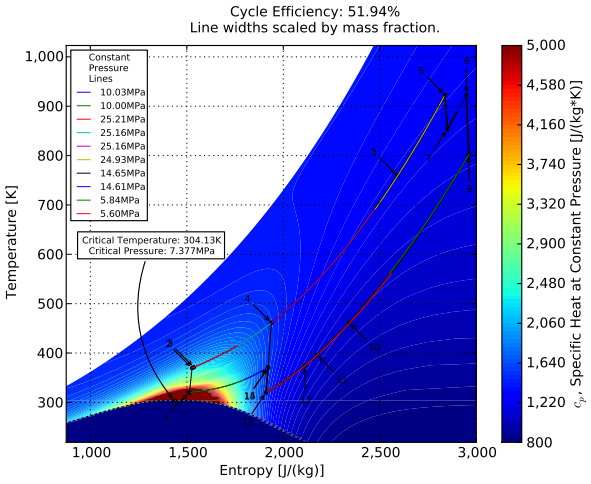

Figure 2: Temperature Entropy Diagram for the Proposed System Layout

The main compressor is the compressor with the minimum entropy at the inlet (point 1). It is possible that a high recompression fraction will be used and the

State Point	Component Inlet	Component Outlet
1	Main Compressor	Cooler
2	Low Temperature Recuperators, High Pressure Side	Main Compressor
3	Medium Temperature Recuperator High Pressure Side	Low Temperature Recuperators, High Pressure Side
4	High Temperature Recuperator High Pressure Side	Medium Temperature Recuperator High Pressure Side, Recompressor
5	Heater High Pressure Side	High Temperature Recuperator High Pressure Side
6	High Pressure Turbines	Heater High Pressure Side
7	Reheater High Pressure Side	High Pressure Turbines
8	Power Turbine	Reheater High Pressure Side
9	High Temperature Recuperator Low Pressure Side	Power Turbine
10	Medium Temperature Recuperator Low Pressure Side	High Temperature Recuperator Low Pressure Side
11	Low Temperature Recuperator Total Fraction Low Pressure Side	Medium Temperature Recuperator Low Pressure Side
12	Cooler Low Pressure Side	Low Temperature Recuperator Total Fraction Low Pressure Side
13	Precompressor	Cooler Low Pressure Side
14	Low Temperature Recuperator Main Fraction Low Pressure Side, Recompressor	Precompressor
15	Cooler Low Pressure Side	Low Temperature Recuperator Main Fraction Low Pressure Side

Table 1: Summary of State Points

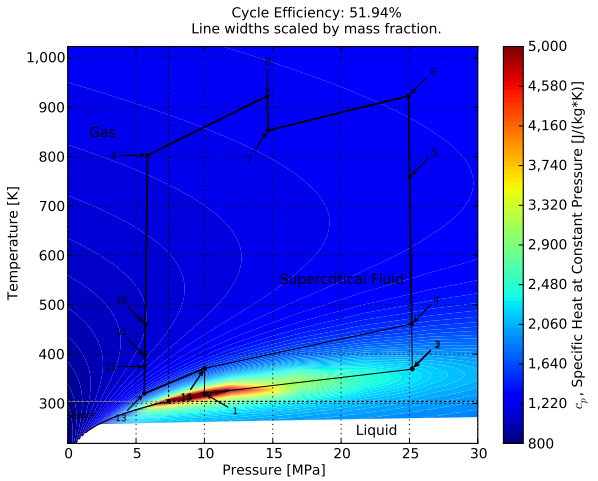

Figure 3: Temperature Pressure Diagram for the Proposed System Layout

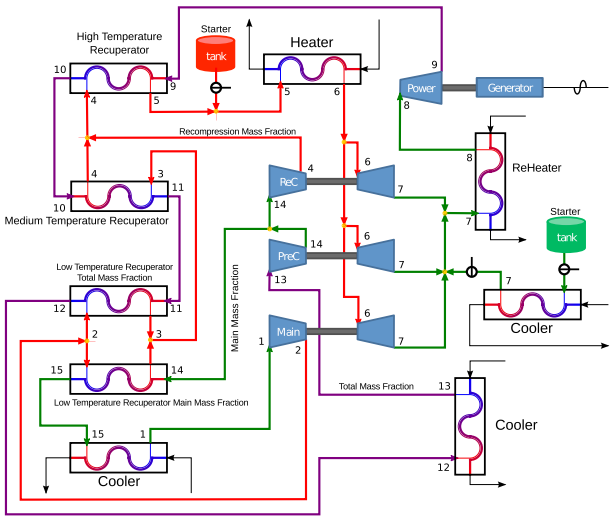

Figure 4: Proposed Supercritical Carbon Dioxide Power Cycle Layout. There are four rotating shafts, three compressors, four turbines, and up to four recuperators.

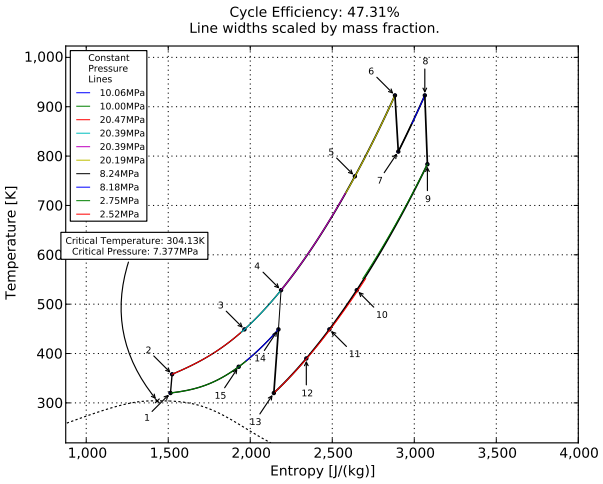

Figure 5: Example System Layout Showing Two Low Temperature Recuperators - Temperature Entropy Diagram

main compressor will actually not have the bulk of the mass flow, but the name will continue to be used. The precompressor (points 13-14) is used to compress the working fluid and can allow for additional recuperation (improved regeneration), helping with the specific heat mismatch between the high and low pressure sides. The use of the precompressor in addition to the main compressor (points 1-2) also allows for more efficient compression overall since the compression portion of the cycle occurs within a lower temperature range (better approximating a Carnot cycle) and there is additional heat rejection (intercooling).

There is a flow split at the exit of the precompressor (point 14) and some mass flow enters a recompressor and the remaining mass flow passes through an additional recuperator, heat rejection heat exchangers and main compressor. The flow then recombines at the exit of the recompressor (point 4). The fraction of the total mass flow rate that enters the recompressor is called the recompression fraction. The purpose of the flow split is because of the specific heat mismatch between the high and low pressure sides. When the specific heat mismatch is too high, much of the low pressure heat cannot be recuperated. In this case, there is additional entropy created in the heat exchanger because the temperature difference between the high and low pressure fluid streams must be greater in order for heat to be able to transfer and because more external heat has to be added to the cycle at lower temperatures. Rather than operate with heat exchangers with a high specific heat mismatch and large entropy generation, some fraction of the fluid is split (the recompression fraction) and recompressed. This results in less mass flow near the critical point on the high pressure side, making the heat capacity (not specific heat capacity) lower. Although the specific enthalpy change (but not necessarily the enthalpy change) in the recompressor is greater than that of the main compressor, making the recompressor's efficiency (and the efficiency of the turbine that powers the recompressor) potentially play a more significant effect on the back work ratio, the benefit gained by better heat capacity matching coupled with a recompression fraction that is not too high can result in overall greater cycle efficiencies by employing a flow split and recompression.

The cycle has three small, high speed turbines which are used to drive the precompressor, recompressor, and main compressor. Each compressor turbine pair is on a different shaft. After the high pressure fluid is heated by the recuperators (points 2-5) and external heat source (points 5-6), the flow is split (point 6) and enters these three turbines. The flow is split rather than each turbine operating in series in order to reduce the mass flow rate through each turbine so that the turbine will have a larger pressure drop and can operate at a lower speed better matched with the compressor it is powering. In order to simplify the design space, the present study does not explore the relative mass flow rates through each turbine and assumes all three turbines have the same isentropic efficiency. After expanding through the turbines (points 6-7), the flow is recombined (point 7) and reheated by the external heat source (points 7-8). After being reheated the fluid then enters a power turbine (points 8-9) which delivers shaft power to the engine's external load (an electrical generator), and is expected to operate at a much lower speed than the 3 smaller turbines. This is believed to be the first formal proposal of such a configuration, and was done so because of the extreme speed difference expected between the power turbine and compressors such that it is not ideal to have a single turbine driving the compressors and electrical generator or alternator. If all are on a single shaft, the design of the turbomachinery can't be optimized very well. The other advantage is that the small turbines and compressors could be placed in containment vessels, eliminating the need for high speed, high pressure rotating seals. The only needed rotating seal would be on the power turbine, which would likely be a larger, slower turbomachine operating at a lower pressure, which would result in a more manageable seal design. The test rigs designed and operated by Sandia National Laboratories were described to have challenges and limitations by utilizing a starter motor/alternator on each shaft, due to speed limitations of the motors and high

pressure, high speed rotating seals[7, 8]. In order for this configuration to work with no starter motors connected to the three smaller turbines, a pressurized tank would be required to do a blow down startup procedure in order for the engine to reach its operating speed. It is also possible that a positive displacement pump may be able to be used in place of a tank in order to temporarily provide flow to the smaller turbines.

There is a high temperature recuperator (points 4-5 and 9-10), medium temperature recuperator (points 3-4 and 10-11), and two low temperature recuperators (points 2-3, 11-12, and 14-15). The low temperature recuperators have an additional flow split on the high pressure side (at point 2) directing flow to the two different heat exchangers and then recombining (point 3). When modeling, this more general configuration was assumed and the mass fraction of this additional flow split was explored. The mass fraction on the high pressure side that was explored was called the ''Low Temperature Recuperator Main Fraction High Pressure Component Mass Fraction'' and represented the mass fraction that was split at point 2 and then went through the heat exchanger which was cooling the main mass fraction flow. The low temperature recuperator cooling the total mass fraction received the complement of the ''Low Temperature Recuperator Main Fraction High Pressure Component Mass Fraction'' on the high pressure side. Figure 5 shows an example of a configuration where two low temperature recuperators are in use. In some cases, one or both of the low temperature recuperators will not exist, and in some cases the medium temperature recuperator also will not exist. Figure 2 is an example configuration where only one low temperature recuperator is in use. The one low temperature recuperator that is in use has a much smaller temperature difference on the high pressure side than the low pressure side due to a higher specific heat on the high pressure side. Also included in Figure 4 are heat rejection heat exchangers. Details related to pressure drop and specific heat of the ambient pressure side of the heat exchanger was not considered in the present analysis and the power required to pump the coolant was considered to be low.

3.2 Computer Code Overview

A Supercritical Carbon Dioxide Power Cycle analysis code was created from scratch using Python [14], NumPy [15], SciPy [16], and matplotlib [17]. Variable fluid properties are utilized (i.e. $h = h(T, p)$, $c_p = c_p(T, p)$, and $s = s(T, p)$) throughout the code. Fluid property data was obtained using REFPROP FORTRAN functions[1] and a forked version of the python-refprop module[18]. A hybrid approach was used to access fluid properties. For commonly accessed properties, property data was populated in advance using REFPROP and stored into RAM for use with an interpolation function. Less commonly used properties are accessed directly from REFPROP as needed. This hybrid approach allowed for an increase in run speed because the interpolation function call was relatively resource expensive, but more efficient at obtaining multiple values simultaneously. Although REFPROP supports many fluids, only carbon dioxide is currently implemented in the present cycle code and all figures shown in the present work are results using carbon dioxide only.

The fluid property functions were setup to accept temperature and pressure (T, p), temperature and entropy (T, s), enthalpy and entropy (h, s), pressure and entropy (p, s), or enthalpy and pressure (h, p) as inputs. From these inputs, temperature, pressure, enthalpy, entropy, density, specific heat at constant pressure, specific heat at constant volume, speed of sound, dynamic viscosity, thermal conductivity, and compressibility factor could be obtained. Because only two inputs were required the code is not yet setup in a general enough way that it can fully function in regions where mixtures of liquids and vapor can coexist in equilibrium (within the liquid vapor dome). The code assumes all fluids are either supercritical fluids or gases. As a result, cycles where condensing may occur are not currently studied. Although liquids should work with the present fluid property lookup technique, they were not considered in order to avoid the chance of a design configuration where some fluid did condense.

The most complicated portion of the code is the real fluid heat exchanger functions. These functions will be discussed in more detail in Section 3.3. Although considerably simpler, functions have also been created to model the turbomachines. The isentropic efficiency for a compressor was defined to be:

$$\eta = \frac{h_{o,ideal} - h_i}{h_o - h_i} \tag{1}$$

where the compressor outlet enthalpy (h_o) can be determined from a known compressor isentropic efficiency (η), pressure ratio (PR_c), and inlet temperature (T_i) and pressure (p_i). The compressor inlet enthalpy (h_i) and entropy (s_i) are evaluated using the fluid property functions using the known temperature and pressure as inputs. The ideal compressor outlet has the same entropy as the compressor inlet. The outlet pressure

for both the ideal and actual compressor outlet is:

$$p_o = p_i * PR_c \tag{2}$$

Using a known pressure and entropy, the ideal compressor outlet enthalpy ($h_{o,ideal}$) can be found using the fluid property functions. With all of these parameters known, the actual compressor outlet enthalpy can be found using the relationship:

$$h_o = \frac{(h_{o,ideal} - h_i)}{\eta} + h_i \tag{3}$$

With a known compressor outlet enthalpy and pressure, the compressor outlet temperature (T_o) could be found using the fluid property functions.

A similar procedure was used for the turbines. The isentropic efficiency of a turbine was defined to be:

$$\eta = \frac{h_i - h_o}{h_i - h_{o,ideal}} \tag{4}$$

The turbine inlet enthalpy (h_i) and entropy (s_i) were known in terms of the inlet (T_i) temperature and pressure (p_i). The isentropic efficiency (η) was also defined. The ideal turbine outlet entropy ($s_{o,ideal}$) was the same as the inlet entropy (s_i). For the high pressure turbines, the actual outlet enthalpy (h_o) was defined based on the energy (W) required to drive the compressors used in the cycle:

$$h_o = h_i - W \tag{5}$$

With a known actual outlet enthalpy and inlet enthalpy, an ideal outlet enthalpy ($h_{o,ideal}$) could be calculated

$$h_{o,ideal} = h_i - \frac{W}{\eta} \tag{6}$$

Using the ideal outlet enthalpy ($h_{o,ideal}$) and entropy ($s_{o,ideal}$), the turbine outlet pressure could be determined using the fluid property functions. The ideal turbine outlet pressure was the same as the actual turbine outlet pressure. Using a known turbine outlet enthalpy and pressure, the turbine outlet temperature and entropy could be found using the fluid property functions.

The power turbine was solved in a slightly different way. Rather than matching a work output, the power turbine needed to match the pressure ratio so that the power turbine outlet pressure equaled precompressor inlet pressure plus the high, medium, and low temperature recuperator pressure drops. The iterative process worked by guessing a pressure ratio in the power turbine and then calculating the turbine work output. The guessed turbine outlet pressure is:

$$p_o = p_i / PR_t \tag{7}$$

With a guessed outlet pressure (p_o) and a known ideal outlet entropy (s_o), a guessed ideal turbine outlet enthalpy ($h_{o,ideal}$) could be found using the fluid property functions. With a guessed ideal turbine outlet enthalpy known, a guessed actual turbine outlet enthalpy could be calculated as

$$h_o = h_i - \eta * (h_i - h_{o,ideal}) \tag{8}$$

and the guessed turbine work could then be calculated

$$W = h_i - h_o \tag{9}$$

With a guessed turbine outlet pressure and enthalpy the fluid property functions could be used to determine the turbine outlet temperature. The initial guess for the power turbine outlet pressure was based upon no pressure loss in the heat exchangers. After a power turbine outlet temperature was guessed, a guessed size of the heat exchangers and pressures drop could be made. With a new guessed heat exchanger pressure drop, a new power turbine outlet pressure guess could be made. The process repeated until the newly guessed pressure drops stopped changing with subsequent iterations. If the change in pressure from iteration to iteration was less than 0.0001% the pressure was considered to be converged. If the change in pressure from iteration to iteration would not decrease below .0001%, the convergence criteria was relaxed to 0.3%. Once a converged turbine outlet pressure was established, the guessed turbine outlet conditions and turbine work were assumed to be the actual values. If the relaxed convergence criteria could not be met, an exception was raised. If the process converged to pressure ratio less than 1, an exception was raised because the engine would not be able to start because more work would be required to drive the compressors and overcome the heat exchanger pressure drops than what was being produced.

This iterative process just described was not managed by a turbine specific function, but rather, was managed by a much larger overall function that laid out the entire cycle using the heat exchanger functions and turbomachinery functions. The main cycle layout function also has the capability to iteratively solve for the other unknown pressures within the cycle, the precompressor inlet pressure and the recompressor outlet pressure. The main cycle layout function coordinated the mass splits in the cycle and ensured all of the component inlet and outlet conditions were in agreement. As was mentioned previously, pumping power for the ambient pressure side of the heaters and coolers are assumed to be low and was not considered in the computer code. The heat source currently modeled is that

of a constant heat flux (i.e. solar) or a highly regenerated combustion system (heater efficiency is assumed to be 100%) where no heat is wasted in the exhaust flow. With these assumption of low pressure drop, very simple functions were created for the heaters and coolers and were called by the main cycle layout function. The main cycle layout function also totaled all of the energy flows and determined a cycle efficiency.

A set of design exploration functions were created to generate a permutation list and run all permutations of the main cycle layout function in parallel. Another set of functions was developed to plot the results of the design exploration, the layout of the cycle, as well as the temperature variation and fluid properties within the heat exchangers. Finally, a set of functions was developed to display and interact with all of this data using a web server and web browser [19].

3.3 Real Fluid Heat Exchangers

Most heat exchangers operate with fluids with nearly constant specific heats and/or are changing phase. Counterflow heat exchangers where both fluids have constant and similar specific heats have a constant and equal slope for the temperature on both the heated and cooled side. Counterflow heat exchangers where the two fluids have constant but dissimilar specific heats are characterized by constant but unequal sloped fluid temperature. Counterflow heat exchangers where the cooled side is condensed and the heated side has a constant specific heat are characterized by a constant temperature on the cooled side and a constant sloped temperature on the heated side. Counterflow heat exchangers where the heated side is vaporized and the cooled side has a constant specific heat are characterized by a constant temperature on the heated side and a constant sloped temperature on the cooled side. For all of these cases, the location of minimum temperature difference between the high and low pressure sides is at an end of the heat exchanger. For the case where the specific heats are constant and similar, the temperature difference is constant throughout the heat exchanger and therefore the location of minimum temperature difference also occurs throughout the entire heat exchanger. The location of minimum temperature difference is sometimes referred to as the pinch point.

Heat exchangers operating with fluids near the critical point possess wildly nonlinear and dissimilar specific heats which dramatically complicates performance analysis. The slope of the fluid temperature is nonlinear and the minimum temperature difference between the heated and cooled fluids may occur in multiple places and not necessarily at the ends of the heat exchanger. Understanding the performance of heat exchanges operating with fluids near the critical point is very important in accurately predicting the performance of real fluid power cycles.

A one dimensional real fluid counterflow heat exchanger solver has been developed as part of the Supercritical Carbon Dioxide Power Cycle analysis code. This one dimensional solver takes into account variable fluid specific heats as well as different mass fractions between the high and low pressure side. The primary purpose of this solver is to understand the impact of the variable specific heat on heat transfer. Forced convection is assumed to be the limiting case where convection is very high and the temperature difference within the fluid boundary layers and heat exchanger solid walls is negligible and the primary cause of the temperature difference within the heat exchanger is due to the variable specific heat mismatch between the two working fluids. Conduction along the length of the heat exchanger is also assumed to be negligible. The case of a heat exchanger with very high forced convection is believed to be a reasonable assumption in the case of Supercritical Carbon Dioxide Power Cycles because the very high pressures result in very high fluid densities that typically lead to very small heat exchanger passages with high convection. These very small passages are feasible because pure carbon dioxide is a fairly inert fluid which will result in minimal scaling of small passages and because carbon dioxide has a relatively low viscosity. Additionally, the manufacturability of heat exchangers with very small passages is becoming a reality through the use of advanced manufacturing techniques.

The pressure drop in the heat exchanger is defined as a linear function of the temperature drop, but this pressure drop is not computed based on any assumed geometry. The slope of this linear function is defined by a coefficient, d. The definition of a pressure drop as a function of temperature allows one to explore the impact of the pressure drop in the heat exchanger on the overall power cycle performance that would be required to achieve this limiting case of high convection. This aids the heat exchanger designer by providing a reference on how important it is to minimize pressure loss in order to achieve the very high forced convection coefficients. The assumption that the pressure drop is a linear function of the temperature drop was used because it is assumed that the length of the heat exchanger will be related to the temperature drop in the heat exchanger and the longer the length of the heat exchanger, the larger the pressure drop. This

assumption could be improved in many ways, but was utilized because of its simplicity and because low system component pressure drops are anticipated.

The specific heat was evaluated for 200 discrete temperatures in the heat exchanger, on both the high and low pressure sides. The ratio of these specific heats between the high and low pressure side was then calculated at each temperature. Information about the relative specific heat between the high and low pressure side was used to help accelerate the solution process. Key information included the average specific heat ratio, temperatures where the specific heat ratio was equal to 1, the average slope of the specific heat ratios, as well as the average concavity of the specific heat ratios. The logic which utilized these qualities of the specific heat ratios aimed to predict the temperature (T_p) where pinching occurred: at the high or low temperature of the heat exchanger, everywhere in the heat exchanger, or in the middle of the heat exchanger (which could be more than one temperature).

Knowing the location of a pinch point was desired because it eliminated one unknown from the problem since both the high and low pressure fluid streams were at approximately the same temperature (based on the assumption of infinitely high convection). With a known temperature where both fluid streams were at the same temperature, the problem reduced to a simple single control volume energy balance with one unknown temperature for cases where the pinching occurred at an inlet or outlet, or two simple control volumes with two unknown temperatures for cases where the pinching occurred in the middle of the heat exchanger.

For the more general case where there were two control volumes, the pressures at the pinch point ($p_{p,Cooled}$ and $p_{p,Heated}$) were defined as

$$p_{p,Cooled} = p_{i,Cooled} - (T_{i,Cooled} - T_p) * d \tag{10}$$

and

$$p_{p,Heated} = p_{i,Heated} - (T_p - T_{i,Heated}) * d \tag{11}$$

where $p_{i,Cooled}$ and $T_{i,Cooled}$ are the inlet pressure on the cooled side and $p_{i,Heated}$ and $T_{i,Heated}$ are the inlet pressure on the heated side. With a known temperature and pressure at the pinch point, the enthalpy on both the heated ($h_{p,Heated}$) and cooled ($h_{p,Cooled}$) side could be found using the fluid property functions. The enthalpy at the inlet on the heated ($h_{i,Heated}$) and cooled ($h_{i,Cooled}$) sides of the heat exchanger could be found using the fluid property functions. The energy balance for the two control volumes described above can be represented by

$$(h_{p,Heated} - h_{i,Heated}) * \dot{m}_{Heated} = (h_{p,Cooled} - h_{o,Cooled}) * \dot{m}_{Cooled} \tag{12}$$

and

$$(h_{o,Heated} - h_{p,Heated}) * \dot{m}_{Heated} = (h_{i,Cooled} - h_{p,Cooled}) * \dot{m}_{Cooled} \tag{13}$$

where $h_{o,Heated}$ and $h_{o,Cooled}$ are the enthalpies at the outlet of the heated and cold side of the heat exchanger. $\dot{m}_{Heated}$ and $\dot{m}_{Cooled}$ are the mass flow rates on the heated and cooled sides. Equations 12 and 15 could then be solved for to find the outlet enthalpies

$$h_{o,Cooled} = h_{p,Cooled} - \frac{(h_{p,Heated} + h_{i,Heated}) * \dot{m}_{Heated}}{\dot{m}_{Cooled}} \tag{14}$$

and

$$h_{o,Heated} = \frac{(h_{i,Cooled} - h_{p,Cooled}) * \dot{m}_{Cooled}}{\dot{m}_{Heated}} + h_{p,Heated} \tag{15}$$

The outlet temperatures on the heated ($T_{o,Heated}$) and cooled ($T_{o,Cooled}$) sides could then be found using the known outlet enthalpies and the outlet pressures using the fluid property functions. If the pinch point was at an endpoint, a similar, but simpler procedure was used because there were less unknowns.

Once all heat exchanger outlet temperatures were calculated, the solution was verified by using the known inlet and outlet temperatures on the low temperature side of the heat exchanger. For each discrete temperature on the low pressure side, a temperature was calculated on the high pressure side using an energy balance of a simple control volume, using previously calculated temperatures on the low temperature side of the control volume. The resulting temperatures on the high and low pressure side were then compared to check for any negative temperature differences, which would indicate a failure of the logic described above to identify the correct heat exchanger pinch point. The newly computed high temperature outlet and inlet temperatures were also compared to those of the original one or two control volume technique. For most scenarios, the logic proved to be successful. Because of some errors, which are believed to be due to the fluid property database as well as the current discretization technique, an error of up to 1.3K was accepted. If the negative temperature difference was more than 1.3K, a trial and error method was utilized in an attempt to identify the correct pinch point location, and the

above process was repeated until an error of less than 1.3K was achieved. If an error less than 1.3 K was not achieved, the heat exchanger function returned an error.

As was mentioned above, the pressure drops in the heat exchangers were defined to be a function of the temperature changes in the heat exchangers. The technique that was just described for finding the heat exchanger outlet temperatures assumed that the outlet pressures were known. Because the temperature changes in the heat exchanger were initially unknown, an iterative process was required in order to determine appropriate pressure drops. An initial guess for the heat exchanger pressure drops was based upon the low temperature inlet/outlet temperatures being equal and the high temperature inlet/outlet temperatures being equal. Temperature changes within the heat exchangers were found using the guessed pressure drops based upon the initially guessed temperature change. With new guessed pressure drops based on calculated heat exchanger temperature changes, the heat exchanger temperature changes were evaluated again using the process described above. The entire process was repeated until the temperature changes and pressure drops in the heat exchangers stopped changing. If the change in inlet/outlet pressures from iteration to iteration was less than 0.0001%, the solution was considered to be converged. If a change in inlet/outlet pressure of less than 0.0001% could not be achieved, the convergence criteria was relaxed to a change in inlet/outlet pressure of 0.3%. If this relaxation was insufficient, the heat exchanger function raised an exception.

It is important to make it clear that no geometry is assumed in this heat exchanger solver and that the purpose of the solver is to aid cycle and heat exchanger designers in understanding the thermodynamic limit of heat exchanger performance due to the variable specific heat mismatch. Because no geometry is assumed, no length dimension is used when plotting the results, but rather, results are presented as a function of the temperature of the cooled fluid stream. The temperature of the cooled fluid stream is related to the length dimension, but no specific relationship is presently assumed. This technique also has not yet been adapted to handle heat exchangers where a fluid is boiling or condensing. A separate web based interface was also created for this heat exchanger solver, which plots specific heats, temperature, and temperature difference for the heated and cooled fluid streams in a heat exchanger [19].

Figure 6 shows an example plot created using the web based interface. The left plot shows the specific heats of both the heated and cooled sides of the heat exchanger. Two specific heats are presented for each fluid stream. $c_{p,Heated}$ and $c_{p,Cooled}$ are based upon the fluid stream's mass flow, and C_{Heated} and C_{Cooled} are based upon mass flow of the cooled fluid stream and are defined in Equations 16 and 17.

$$C_{Heated} = c_{p,Heated} * \frac{\dot{m}_{Heated}}{\dot{m}_{Cooled}} \tag{16}$$

$$C_{Cooled} = c_{p,Cooled} * \frac{\dot{m}_{Cooled}}{\dot{m}_{Cooled}} = c_{p,Cooled} \tag{17}$$

C_{Heated} and C_{Cooled} are presented so that heat capacity can be compared for heat exchangers with different mass flow rates on the heated and cooled side, which can happen in cycles with recompression. It is important to note that $c_{p,Cooled}$ and C_{Cooled} have the same values and as a result, the curves are overlapping. One can see a highly non-linear and dissimilar c_p for both the heated and cooled sides of the heat exchanger. In the example configuration shown, C is still dissimilar between the heated and cooled sides of the heat exchanger.

An important metric for evaluating heat exchanger performance is the heat exchanger's effectiveness (ϵ), which is defined as

$$\begin{aligned}\epsilon &= \frac{(h_{o,Heated} - h_{i,Heated}) * \dot{m}_{Heated}}{\boldsymbol{min}((h_{o,max,Heated} - h_{i,Heated}) * \dot{m}_{Heated}, \\ &\qquad (h_{i,Cooled} - h_{o,min,Cooled}) * \dot{m}_{Cooled})} \\ &= \frac{(h_{i,Cooled} - h_{o,Cooled}) * \dot{m}_{Cooled}}{\boldsymbol{min}((h_{o,max,Heated} - h_{i,Heated}) * \dot{m}_{Heated}, \\ &\qquad (h_{i,Cooled} - h_{o,min,Cooled}) * \dot{m}_{Cooled})}\end{aligned} \tag{18}$$

where $h_{o,max,Heated}$ is the maximum enthalpy the heated side fluid could have if the heated side outlet could reach the temperature of the cooled side inlet ($T_{i,Cooled}$) and $h_{o,min,Cooled}$ is the minimum enthalpy the cooled side fluid could have if the cooled side outlet could reach the temperature of the heated side inlet ($T_{i,Heated}$). Heat exchanger effectiveness helps one assess how much of the heat that *can* be transferred *is* transferred. For the present study, the heat exchanger effectiveness was assumed to be 100% based on the assumption of very high convection and all heat that can be transferred is assumed to be transferred. An important metric to also consider is the maximum amount of heat that *can* transferred compared to the maximum one may *want* to transfer from either the heated or cooled fluids. In the case of supercritical carbon dioxide power cycle design, one always wants to transfer as much heat as possible, but because of the specific heat mismatch,

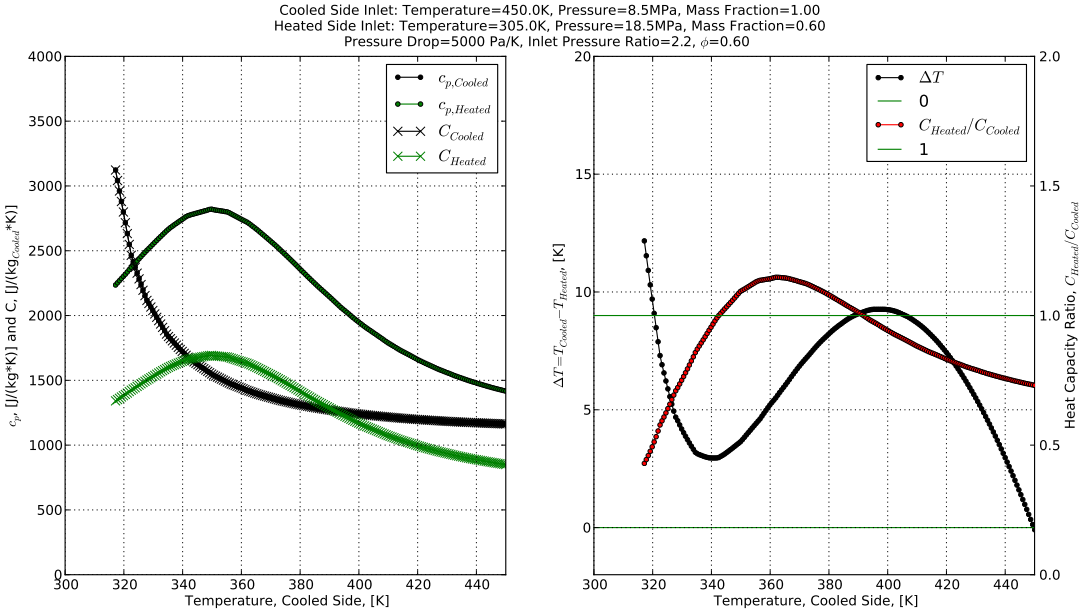

Figure 6: Sample Heat Exchanger Solution

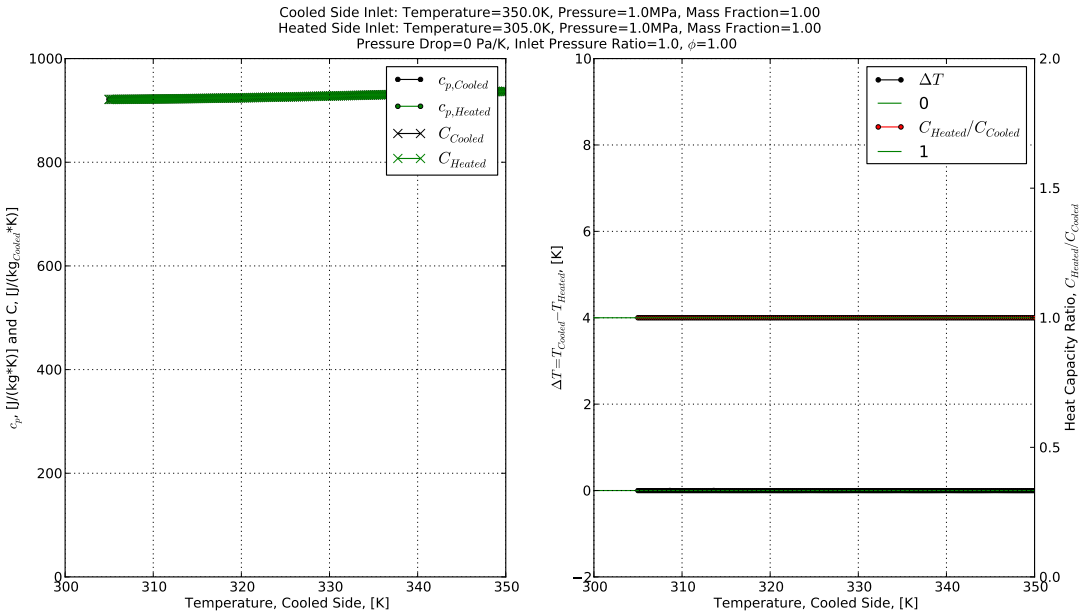

Figure 7: Sample heat exchanger solution with nearly constant and similar specific heats

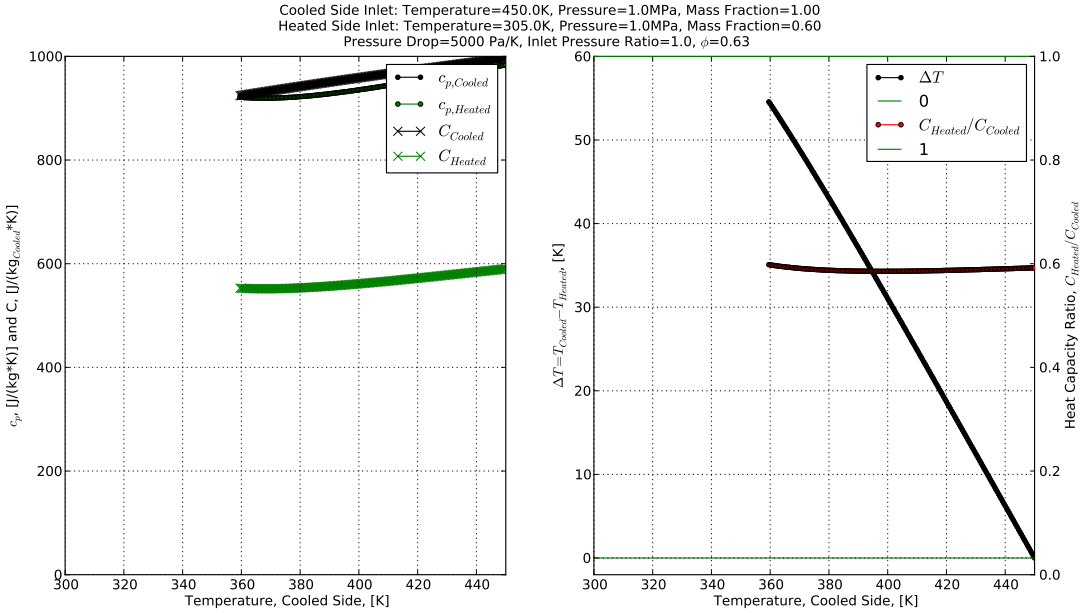

Figure 8: Sample heat exchanger solution with nearly constant but dissimilar heat capacities

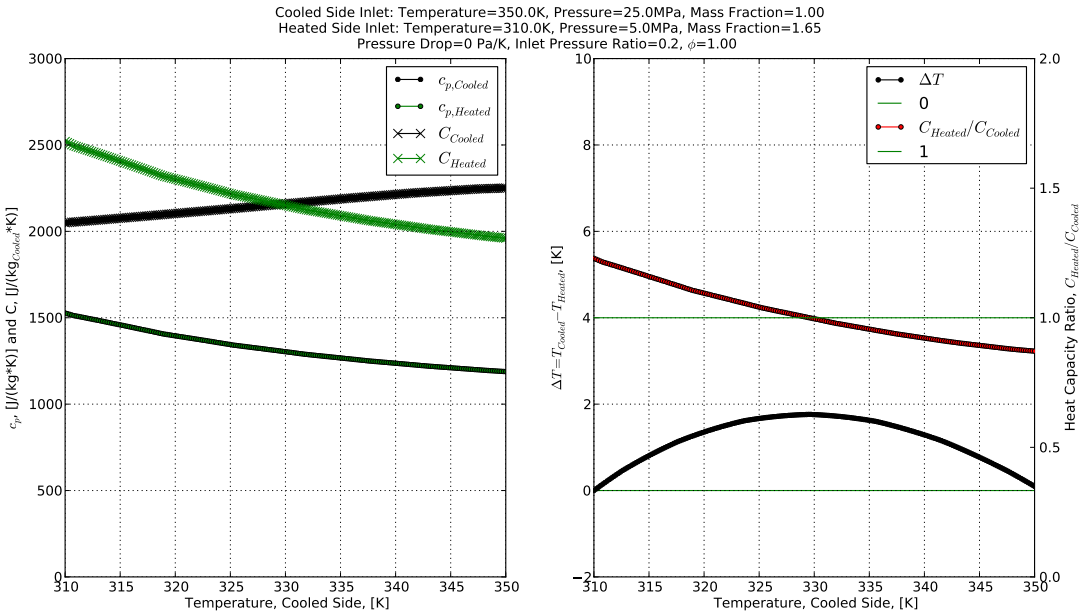

Figure 9: Sample heat exchanger solution where the heat exchanger is pinched at both ends

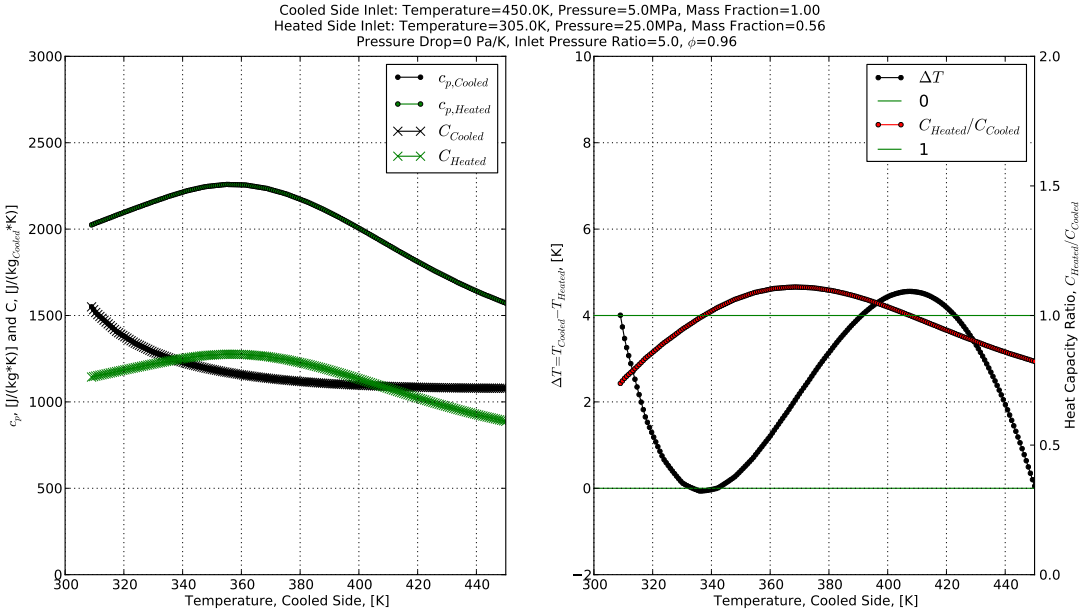

Figure 10: Sample heat exchanger solution where the heat exchanger is pinched in the middle and at the high temperature end

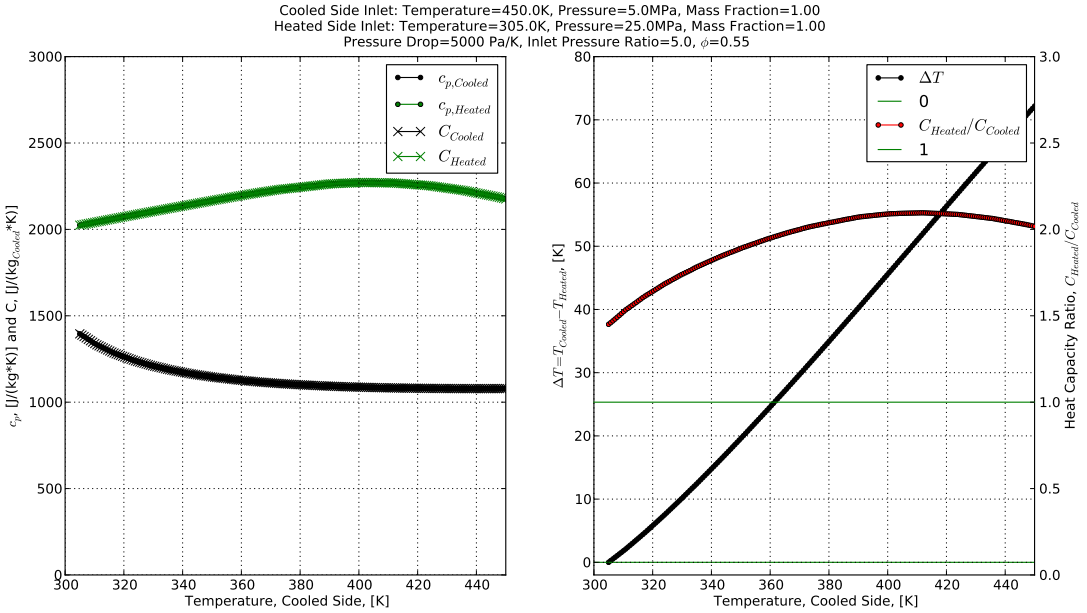

Figure 11: Sample heat exchanger solution where the heat exchanger is pinched only at the low temperature end

there isn't always enough heat available to be transferred on the cooled side and there isn't always enough heat that can be accepted on the heated side. No term is known to identify this metric, so a new name will be given as the ''Fraction of Desired Heat Transferred'' and will be associated with the symbol ϕ and defined as

$$\begin{aligned}\phi &= \frac{(h_{o,Heated} - h_{i,Heated}) * \dot{m}_{Heated}}{\boldsymbol{max}\big((h_{o,max,Heated} - h_{i,Heated}) * \dot{m}_{Heated}, \\ &\qquad (h_{i,Cooled} - h_{o,min,Cooled}) * \dot{m}_{Cooled}\big)} \\ &= \frac{(h_{i,Cooled} - h_{o,Cooled}) * \dot{m}_{Cooled}}{\boldsymbol{max}\big((h_{o,max,Heated} - h_{i,Heated}) * \dot{m}_{Heated}, \\ (h_{i,Cooled} - h_{o,min,Cooled}) * \dot{m}_{Cooled}\big)}\end{aligned} \quad (19)$$

This new metric can be used to assess how well the specific heats are matched between the heated and the cooled sides. In Figure 6 the ''Fraction of Desired Heat Transferred'' is 0.60, which means that 60% of the heat that one would like to accept on the heated side could be transferred to the heated side, or 60% of the heat that one would like to have available on the cooled side to accept on the heated side could be transferred to the heated side.

In the right plot of Figure 6, the temperature difference (ΔT) and ratio of specific heats (C_{Heated}/C_{Cooled}) is presented. Two reference horizontal lines are presented for the temperature difference and ratio of specific heats at 0 and 1 respectively. The reference line at 0 is presented along with a slightly negative scale in order to assess the potential error in the solution that is described above. The reference line for a specific heat ratio of 1 is presented in order to illustrate clearly how the heated and cooled sides relative specific heat is changing and which fluid stream has a greater specific heat. The relative specific heats are wildly changing in this particular solution and the temperature difference as a result also changes dramatically within the heat exchanger. It's also important to note in this particular example that the temperature difference changes concavity within the heat exchanger, and the temperature difference is close to zero at one local minima and approximately zero at the absolute minima.

In addition to the example solution shown in Figure 6, there are several other example solutions that demonstrate important heat exchanger characteristics. Figure 7 shows a heat exchanger with nearly constant and similar specific heats with similar mass flow rates on both the heated and cooled sides. In this example the temperature difference between the heated and cooled sides is constant and minimum throughout the heat exchanger (it is pinched everywhere). The specific heats of both sides are very well matched and the maximum amount of heat that can be transferred is. Figure 7 is an example well below the critical pressure, so it is not applicable to supercritical carbon dioxide power cycles, however, it is an important case in understanding the impact of specific heats on heat exchanger performance.

Figure 8 shows an example heat exchanger solution where the specific heats are nearly constant (the same pressure as the case in Figure 7), but the mass fractions are different so the heat capacities between the heated and cooled sides are different. In this case the heat capacity on the heated side is always lower than the cooled side. Within the operating temperature range defined by the heat exchanger heated and cooled side inlets, there will not be enough heat capacity on the heated side in order to accept all the heat from the cooled side and the cooled side outlet will never reach the inlet temperature of the heated side (the ''Fraction of Desired Heat Transferred'' is 0.63). The temperature difference varies linearly within the heat exchanger and the location of minimum temperature difference (the pinch point) is at the high temperature end only.

Figure 9 shows an example heat exchanger solution where the location of minimum temperature difference (pinch point) occurs at both ends. In this example the specific heats are dissimilar and varying. This particular case is also not applicable to supercritical carbon dioxide power cycles because the heated side is a lower pressure than the cooled side, however, it illustrates a vary interesting solution which helps to understand heat exchangers with nonlinear and dissimilar specific heats. In this case the mass fraction was adjusted so that the average heat capacities of the heated and cooled sides are well matched. The heat capacity ratio within the heat exchanger changes from greater than one at the low temperature end of the heat exchanger to less than one at the high temperature end of the heat exchanger. The temperature difference within the heat exchanger is still fairly low away from the ends.

In Figure 10 a heat exchanger solution is shown where a pinch point exists at both the high temperature end and in the middle of the heat exchanger. The temperatures and pressures are representative of a heat exchanger operating in a supercritical carbon dioxide power cycle. The specific heat capacities are nonlinear and dissimilar. The mass fraction has been adjusted so that the average heat capacities are nearly the same, which causes the solution to have low temperature differences throughout the heat exchanger. This example points out that the pinch point is not necessarily the problem with heat exchangers in supercritical carbon dioxide cycles. The heat exchanger

has two pinch points but still has a low temperature difference everywhere so nearly all of the heat from the cooled side is transferred to the heated side (the ''Fraction of Desired Heat Transferred'' is 0.96). Pinch points may be unusual in heat exchangers with highly nonlinear and dissimilar specific heats, but they are not the problem, just a distinct feature. The location of the pinch point and the temperature away from the pinch point may help to indicate how good or bad the heat capacity match is between the heated and cooled sides.

A case where the heated side specific heat capacity (and heat capacity) is always higher on the heated side than the cooled side is shown in Figure 11. In this case the heat exchanger relative heat capacities is always changing within the heat exchanger, but because the heat capacity is always higher on the heated side, the pinch point is only at the low temperature end and the temperature difference is very high at the high temperature end of the heat exchanger. Because the heat capacity on the cooled side is lower, the heated side will never reach the inlet temperature of the cooled side (the ''Fraction of Desired Heat Transferred'' is 0.55). This case is an example where the single pinch point at the low temperature end clearly indicates that the heat capacity is much higher on the heated side than the cooled side. It's important to reiterate however that the pinch point itself is not the problem, the heat capacity mismatch is the problem.

All of these example heat exchanger solutions demonstrate some distinct characteristics of heat exchangers with constant, varying, similar, and dissimilar heat capacities. The heat exchanger performance plays a very important part in the performance of a supercritical carbon dioxide power cycle. It's also important to note that real heat exchangers will actually have some non-zero minimum temperature difference and this minimum amount is because the heat exchanger can't have an unlimited length and too high of a pressure drop. The present results are still useful because they provide a rapid solution and clearly isolate the required temperature difference due to specific heat mismatch. If the heat exchanger designer can identify regions where a temperature difference is required due to specific heat match, then forced convection coefficient does not necessarily have to be as high in those regions of the heat exchanger and the heat exchanger designer can harness that temperature difference rather than requiring high convection (which typically results in a higher pressure drop). This approach may result in more complex heat exchanger geometry, but could result in lower entropy production in the heat exchangers.

3.4 Cycle Simulation

Inputs of the cycle simulation include maximum temperature, minimum temperature, compressor pressure ratios, turbomachinery component efficiencies, heat exchanger pressure drop, main compressor inlet pressure, and mass fraction for flow splits. An iterative procedure was utilized to find the unknown pressure drop between states 15 and 1 (the Main Fraction Cooler), the ReCompressor Pressure Ratio, and the Power Turbine Pressure ratio. Although an input variable, the linear pressure drop vs temperature drop constant was fixed to the same value for all heat exchangers in the cycle. Individual heat exchangers currently are not able to have different pressure drop constants. The cycle code presently does not include the ability to handle mixing of fluids of different temperatures where the flow is recombined. In order to ensure temperatures were equal when the flow was recombined, some small heaters and coolers were added if necessary on the high and low pressure sides at the inlet or outlet of the the heat exchanger. It is also important to note that only on-design conditions were studied. The code is currently not able to perform transient simulations or off-design studies at this time.

3.5 Design Exploration

A design explorer was developed to run the Supercritical Carbon Dioxide Power Cycle analysis code with many different input combinations. The design explorer was developed in such a way that the design space could be explored in parallel by running the Supercritical Carbon Dioxide Power Cycle analysis code on multiple processors simultaneously. The code can use as many processors as are available on a single machine. Some effort was conducted to run different batches of permutations on different machines, however, this functionality was abandoned because of the increased complexity of using multiple machines, and the dramatic increase in the number of processors available on a single machine recently. A 48 processor machine was used for the present study.

In order to effectively eliminate some components such as a low temperature recuperator, the precompressor and/or the recompressor from the system, the ''Low Temperature Recuperator Main Fraction High Pressure Component Mass Fraction'' could be set to 0 or 1, the precompressor pressure ratio could be set to a pressure ratio of 1 and the recompression fraction

could be set to 0 or 1.

It's important to note that although the results of the design exploration process can be used to explore optimal system layouts, the approach was not used just for the purpose of identifying a single optimal solution. Although the methodology utilized is fairly in depth, the level of complexity of assessing a true optimal solution is significant. With such a new type of technology, economic, control, and safety concerns for example are difficult to formally and accurately formulate. By exploring the design space completely, rather than using a more efficient adaptive optimization algorithm, engineering judgment can be more appropriately applied to the results through the use of easy to use visualization tools.

4 Results

Two separate runs were conducted in order to explore a broad range of each parameter as well as a refinement of key parameters. Tables 2 and 3 provide a summary of the range and resolution of the parameters studied in both runs, as well as the value plotted. Parameters where the value plotted is indicated to be ''Optimal'' mean that the optimal value is plotted based on the plotting constraints of the other parameters (either fixed or optimal). For plots where a variable is on an axis, the value plotted parameter is not relevant because all values are plotted. Parameters where ''Optimal'' is indicated use the optimal value based on the each value of the parameter on the axes. The first run surveyed 13 parameters and the total number of permutations was 20,155,392. This dataset is called ''Dataset I''. Due to the large number of parameters explored, the range and resolution of each parameter was limited, and a second exploration was conducted. The second exploration focused just on 5 parameters, PreCompressor Pressure Ratio, Main Compressor Pressure Ratio, Recompression Fraction, Low Temperature Recuperator Main Fraction High Pressure Component Mass Fraction, and Main Compressor Inlet Pressure, which resulted in a total of 1,800,000 permutations. The remaining parameters were fixed to values which are assumed to be reasonably attainable component efficiencies. This dataset is called ''Dataset II''.

Extensive efforts were taken to ensure that the heat exchanger and main cycle portions of the code were written as general as possible, however, with a very large design space being explored, it was difficult to ensure every permutation could be solved successfully. Many checks were incorporated into the code to ensure laws of thermodynamics were not being violated in any solution. If any laws of thermodynamics were violated or problems achieving a solution, an exception was raised, the permutation would be aborted, and the efficiency was set to -1 for that permutation as a way of marking it as an unsolvable permutation. Contour plots have a minimum efficiency of 0.30 (30%) presented, and everything less than 0.30 is clipped (appears white instead of blue). Any efficiency less than 0.30 is essentially ignored so that these unsolvable permutations are not considered. For Dataset I, 3.7% of the permutations were unsolvable, and for Dataset II, 5.2% of the permutations were unsolvable.

Selected results of the design exploration can be viewed in Figures 13-19 and the entire dataset can be manipulated and viewed using the web based user interface that was developed as part of the Supercritical Carbon Dioxide Power Cycle analysis code[19]. A screenshot of this web based user interface can be seen in Figure 12. All Figures in this section, as well as Figures 2, 3, 5, and 6 were created using the web based user interface, and utilized the high resolution PDF figure download feature. Contour plots in this section include dots overlayed over the contour. These dots indicate the data points and all contour values in between the dots have been interpolated.

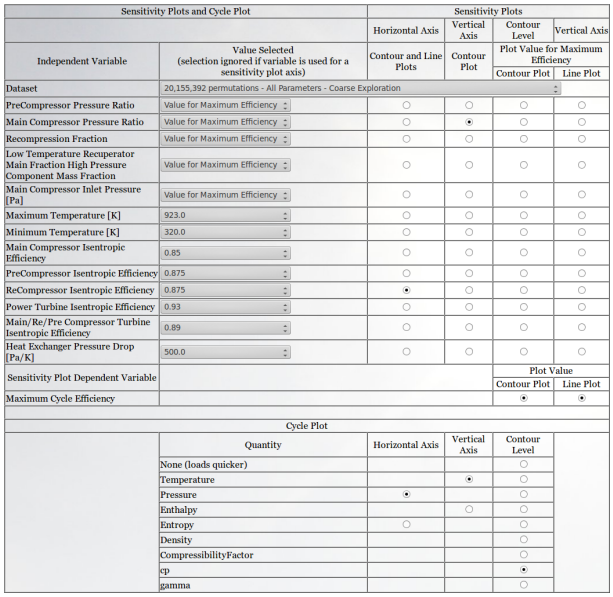

Figure 12: Web Based Graphical User Interface[19]

Figures 13-14d were generated using ''Dataset I''. Figures 13-14b show the sensitivity of the cycle efficiency on the minimum and maximum cycle temperatures. Within the limited range and resolution studied (three high and three low temperatures), the dependency of the cycle efficiency on the minimum

Parameter	Minimum	Maximum	Number of Values	Value Plotted
PreCompressor Pressure Ratio	1.0	4.0	6	Optimal
Main Compressor Pressure Ratio	1.1	4.1	6	Optimal
Recompression Fraction	0.000	0.991	4	Optimal
Low Temperature Recuperator Main Fraction High Pressure Component Mass Fraction	0.001	0.991	4	Optimal
Main Compressor Inlet Pressure	6 MPa	10 MPa	6	Optimal
Maximum Temperature	798K	923K	3	923K
Minimum Temperature	320K	333K	3	320K
Main Compressor Isentropic Efficiency	0.75	1.00	4	0.85
PreCompressor Isentropic Efficiency	0.80	0.95	3	0.875
ReCompressor Isentropic Efficiency	0.80	0.95	3	0.875
Power Turbine Isentropic Efficiency	0.89	0.93	3	0.93
Main/Re/Pre Compressor Turbine Isentropic Efficiency	0.84	0.89	3	0.89
Heat Exchanger Pressure Drop	500 Pa/K	0 Pa/K	2	500 Pa/K

Table 2: Dataset I - 20,155,392 permutations - All Parameters - Coarse Exploration

Parameter	Minimum	Maximum	Number of Values	Value Plotted
PreCompressor Pressure Ratio	1.0	4.0	20	Optimal
Main Compressor Pressure Ratio	1.1	4.1	20	Optimal
Recompression Fraction	0.000	0.991	15	Optimal
Low Temperature Recuperator Main Fraction High Pressure Component Mass Fraction	0.001	0.991	15	Optimal
Main Compressor Inlet Pressure	6 MPa	10 MPa	20	Optimal
Maximum Temperature	923K	923K	1	923K
Minimum Temperature	320K	320K	1	320K
Main Compressor Isentropic Efficiency	0.85	0.85	1	0.85
PreCompressor Isentropic Efficiency	0.875	0.875	1	0.875
ReCompressor Isentropic Efficiency	0.875	0.875	1	0.875
Power Turbine Isentropic Efficiency	0.93	0.93	1	0.93
Main/Re/Pre Compressor Turbine Isentropic Efficiency	0.89	0.89	1	0.89
Heat Exchanger Pressure Drop	500 Pa/K	500 Pa/K	1	500 Pa/K

Table 3: Dataset II - 1,800,000 permutations - Fixed Component Efficiencies and Max/Min Temp, Other Parameters Refined

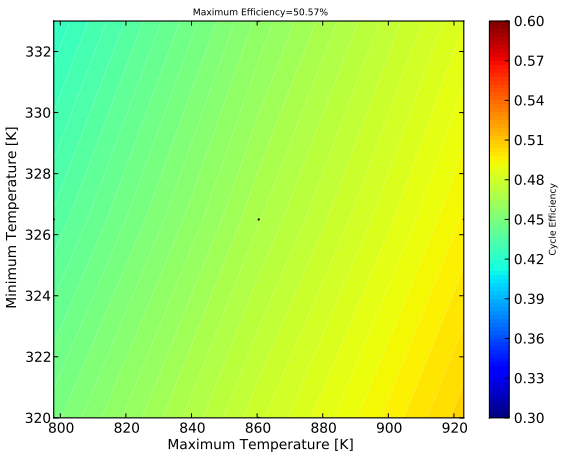

Figure 13: Cycle Efficiency vs Maximum and Minimum Temperature

and maximum temperatures appears to be fairly linear. Figure 14c shows the cycle efficiency's sensitivity to the main compressor's isentropic efficiency. There is some non-linearity evident using the 4 different main compressor isentropic efficiencies that were considered. A larger range and resolution may be preferred in order to better assess the importance of the main compressor's efficiency because it may be desired to use a positive displacement device for some demonstration efforts since the main compressor is expected to be the most difficult turbomachinery design to perfect. The cycle efficiency vs the recompressor isentropic efficiency is shown in Figure 14d. With the limited range and resolution shown, the cycle efficiency appears to be fairly linear with respect to recompressor isentropic efficiency.

Figures 15-19 were generated using ''Dataset II''. The parameters that were not fixed were explored at a fairly high resolution. Figure 15 shows cycle efficiency vs main compressor and precompressor pressure ratios. The maximum cycle efficiency, using the constraints listed in Table 3 in the column ''Value Plotted'' is 51.94%. A Carnot cycle with a maximum temperature of 923K (650°C) and a minimum temperature of 320K (47°C) would have an efficiency of 65.33%. This indicates that the proposed cycle layout may be able to achieve efficiencies of 79.5% of a Carnot cycle efficiency. As is shown in Table 3, there are 20 precompressor pressure ratios and 20 main compressor pressure ratios considered. Observing the results from Figure 15 indicates an even higher exploration range should actually be used because there are some noticeable plotting artifacts in regions with high gradients. At least two local maxima are evident in Figure 15. The same plot, when viewed using the web based interface for ''Dataset I'', which has a lower resolution for the precompressor and main compressor pressure ratios, also shows two local maxima, although at different locations due to plotting artifacts and interpolation errors in regions with high gradients. The main take aways from Figure 15 are that eliminating one of the compressors (i.e. the condition where pressure ratio is 1) will result in a fairly significant reduction in overall cycle efficiency, and that when both compressors are used, there is a wide range of combinations of precompressor and main compressor pressure ratios.

Figure 16 shows the optimal recompression fraction at each precompressor and main compressor pressure ratio. Comparing to Figure 15, the variation of the optimal recompression fraction, near the region of high cycle efficiency, appears to be significant. Because the cycle code in its current form does not allow for the precompressor and main compressor inlet temperatures to be different, as the precompressor pressure ratio or main compressor pressure ratio approach 1, the recompression fraction has no meaning. Therefor values of recompression fraction at pressure ratios of 1 should be ignored (for example, the red vertical region on the left portion of Figure 16).

Figure 17 shows the cycle efficiency vs recompression fraction. For much of the design space, the optimal recompression fraction is between approximately 0.40 and 0.80. It is important to note when comparing Figure 17 to Figures 15 and 16 that the same pressure ratios could be used for multiple recompression fractions in Figure 17.

Figure 18 shows the variation in optimal Low Temperature Recuperator Main Fraction High Pressure Component Mass Fraction vs precompressor and main compressor pressure ratios. For much of the design space, the elimination of one of the low temperature recuperator would be possible. This is particularly true because the regions of pressure ratios where a second low temperature recuperator would be useful are pressure ratios where the cycle efficiency is already lower anyway.

Figure 19 shows that the cycle efficiency increases as the main compressor inlet pressure increases, and that the design exploration should be expanded to higher main compressor inlet pressures in order to locate the optimal main compressor inlet pressure. It is important to note, however, that the present study does not consider the increased design complexities of higher system operating pressures. A more rigorous optimization coupled with costs may locate a different optimal main compressor inlet pressure.

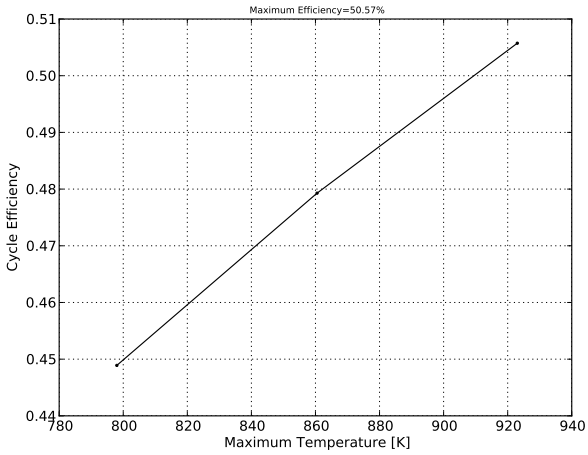

(a) Cycle Efficiency vs Max Temperature

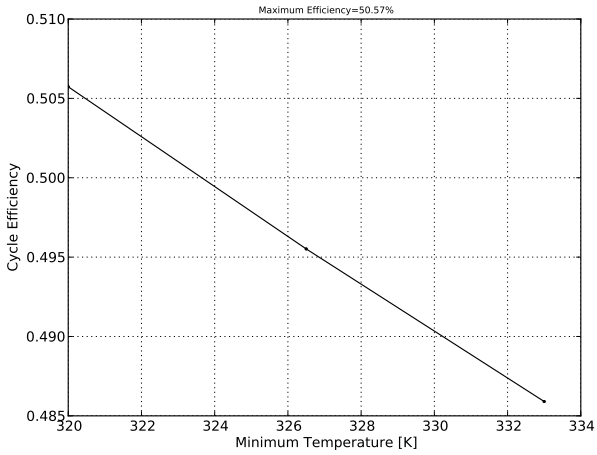

(b) Cycle Efficiency vs Min Temperature

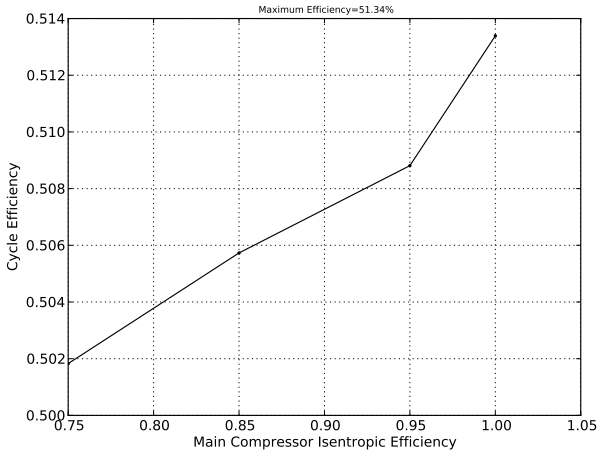

(c) Cycle Efficiency vs Main Compressor Efficiency

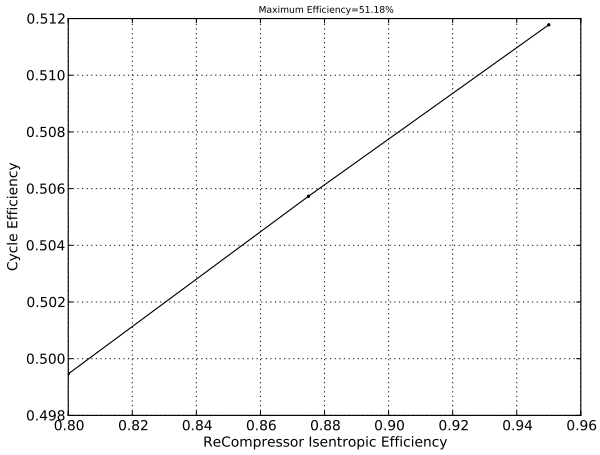

(d) Cycle Efficiency vs ReCompressor Efficiency

Figure 14

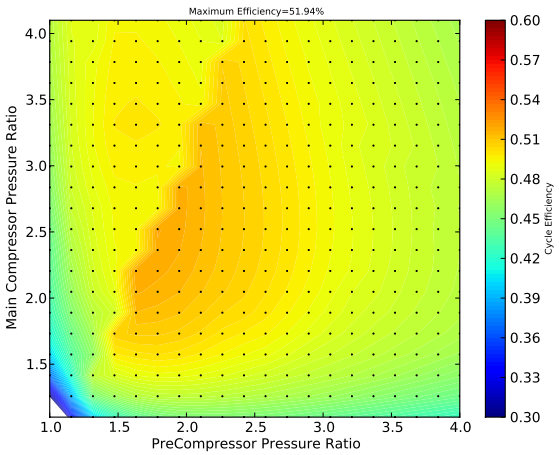

Figure 15: Cycle Efficiency vs PreCompressor and Main Compressor Pressure Ratios

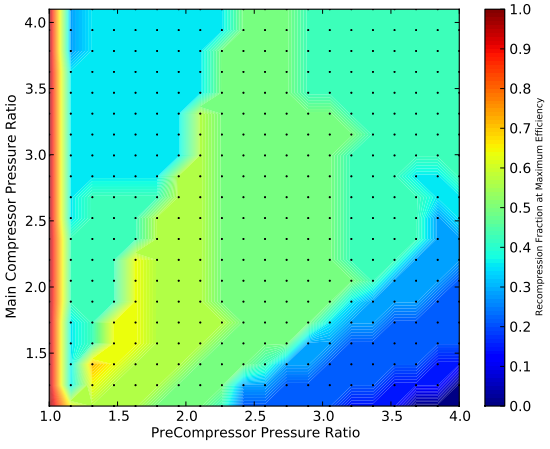

Figure 16: ReCompression Fraction at Optimal Cycle Efficiency vs PreCompressor and Main Compressor Pressure Ratios

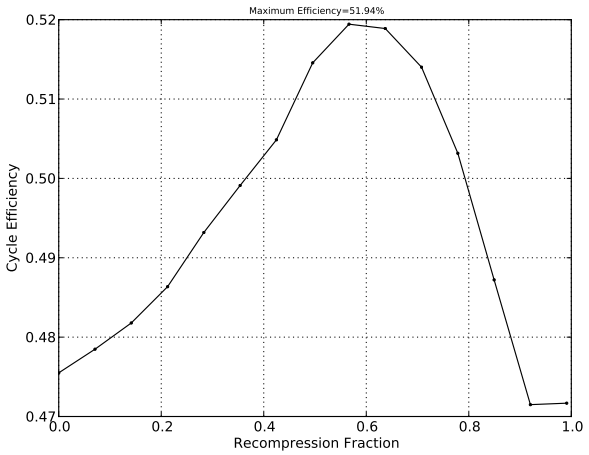

Figure 17: Cycle Efficiency vs ReCompression Fraction

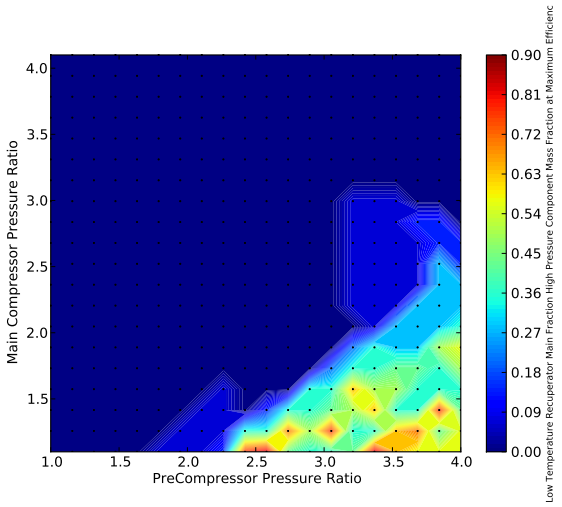

Figure 18: Low Temperature Recuperator Main Fraction High Pressure Component Mass Fraction at Optimal Cycle Efficiency vs PreCompressor and Main Compressor Pressure Ratios

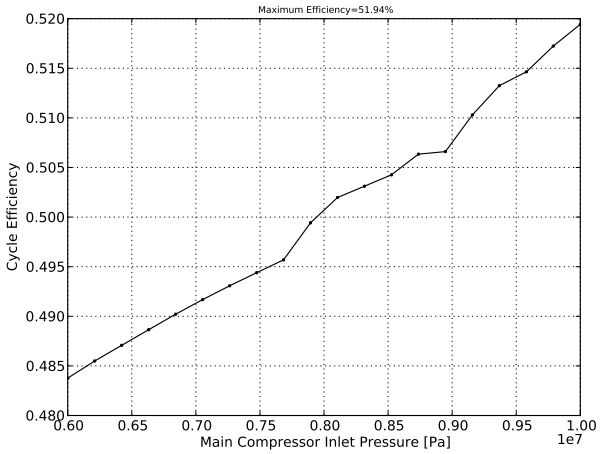

Figure 19: Cycle Efficiency vs Main Compressor Inlet Pressure

5 Conclusions and Future Work

Supercritical CO_2 Power Cycles have the potential for improvements in efficiency over traditional power cycles or traditional combined cycle power plants, at a dramatically reduced system size. However, the highly nonlinear fluid properties present significant challenges in cycle and component design. The present work indicates that a cycle efficiency of 51.94% may be achievable with a maximum heat source temperature of 923K (650°C) and a minimum coolant temperature of 320K (47°C). At 79.5% of the efficiency of a Carnot cycle, this cycle is approaching the thermodynamic limits of a heat engine.

A new system layout has been presented which may help to eliminate some of the design challenges with supercritical carbon dioxide engines. The present work demonstrates a cycle analysis code that was written from scratch specifically to explore a wide range of design parameters for the proposed layout. The web based visualization tool provides a level of insight and interactivity not possible in a traditional static document. This visualization and interactivity helps to better direct the design, testing, and commercialization plan for supercritical carbon dioxide power cycles, and better establish the benefits of systems of different complexities. Although this work is fairly extensive, there is still much to be done to improve the overall picture of the Supercritical Carbon Dioxide Power Cycle design space.

Limitations of the present code include the lack of ability to model cycles below the critical temperature (condensing cycles) where a discontinuous change in phase and two phase region may exist. The code could also be improved to incorporate more realism in the real fluid heat exchangers by accounting for an additional temperature gradient in the fluids' thermal boundary layers and the heat exchangers solid walls. The very low minimum temperature difference in the heat exchangers is expected to slightly over predict the cycle efficiency and under predict the ideal recompression fraction. The pressure drop formulation in the heat exchangers could also be improved and individual relationships applied to different heat exchangers. The code is presently limited such that the precompressor inlet temperature must be equal to the main compressor inlet temperature, and further flexibility could be incorporated to allow for this parameter to be changed independently. The code could also allow for different turbomachinery efficiencies for the turbines that power the compressors and a selectable mass flow split between these turbines that operate

in parallel. The design space explored mostly utilizes a uniformly spaced grid for each parameter. Based on the present results, a non uniformly spaced grid could be harnessed and the design space explored in more detail. The code could be expanded to allow for off-design, as well as transient simulations. Fluid specific heat, pressure drop and pumping power of the atmospheric pressure side of the heat exchangers that transfer heat to and from the engine is currently not rigorously addressed. The code could also be expanded such that the coupled engine cycle efficiency as well as utilization of the heat source are explored and optimized. The present code currently assumes that the heat source is completely utilized and no high temperature heat is unused. Understanding the impact of the heat source on the optimal cycle design and the overall system efficiency is critical in applying such a cycle with fossil fuels such as coal and natural gas, as well as a replacement for a steam turbine in a combined cycle power plant. An estimated system cost could also be computed and the cycle efficiency plotted vs estimated system cost. Finally, the cycle could also be improved to allow for different pure fluids as well as mixtures of fluids, as well as incorporate CoolProp[20], a free, open source, modern fluid property database instead of REFPROP. In addition to improving the cycle code, the web based graphical user interface can be enhanced to allow for plotting dependent variables vs dependent variables, computing and plotting of derivatives, higher speed rendering of the thermodynamic state diagrams, overlaying contour lines of multiple variables on the same plot, multiple axis on the line plots, among other possible features.

References

[1] National Institute of Standards and Standard Reference Data Program Technology. NIST Standard Reference Database 23: Reference Fluid Thermodynamic and Transport Properties-REFPROP.

[2] Sulzer. Verfahren zur Erzeugung von Arbeit aus Warme, 1948. Swiss Patent 269 599.

[3] G Angelino. Perspectives for the liquid phase compression gas turbine. *Journal of Engineering for Gas Turbines and Power*, 89(2):229--236, 1967.

[4] G Angelino. Carbon dioxide condensation cycles for power production. *Journal of Engineering for Gas Turbines and Power*, 90(3):287--295, 1968.

[5] Ernest G Feher. The supercritical thermodynamic power cycle. *Energy conversion*, 8(2):85--90, 1968.

[6] V. Dostal. *A Supercritical Carbon Dioxide Cycle for Next Generation Nuclear Reactors*. PhD thesis, Massachusetts Institute of Technology, Dept. of Nuclear Engineering, 2004.

[7] Steven A. Wright, Tom M. Conboy, and Gary E. Rochau. Break-even Power Transients for two Simple Recuperated S-CO_2 Brayton Cycle Test Configurations. SCO_2 Power Cycle Symposium, May 2011.

[8] Steven A Wright, Ross F Radel, Milton E Vernon, Gary E Rochau, and Paul S Pickard. Operation and Analysis of a Supercritical CO2 Brayton Cycle. SANDIA REPORT, SAND2010-0171, Advanced Nuclear Concepts Department, Sandia National Laboratories, Albuquerque, New Mexico, September 2010.

[9] Kenneth J Kimball, Kevin D Rahner, Joseph P Nehrbauer, and Eric M Clementoni. Supercritical Carbon Dioxide Brayton Cycle Development Overview. In *ASME Turbo Expo 2013: Turbine Technical Conference and Exposition*. American Society of Mechanical Engineers, June 2013.

[10] Echogen Power Systems, LLC. Our Story. `http://www.echogen.com/about/our-story/` Accessed: February 22^{nd}, 2014.

[11] Energy Department Announces New Concentrating Solar Power Technology Investments to American Industry, Universities. `http://energy.gov/articles/energy-department-announces-new-concentrating-solar-power-technology-investments-american`.

[12] SunShot CSP R&D 2012, June 12, 2012. `http://www1.eere.energy.gov/solar/pdfs/csp_rd_awardees_2012.pdf`.

[13] Concentrating Solar Power SunShot Research and Development. `http://energy.gov/eere/sunshot/concentrating-solar-power-sunshot-research-and-development`.

[14] Python. `https://www.python.org/`.

[15] NumPy. `http://www.numpy.org/`.

[16] SciPy. http://scipy.org/.

[17] matplotlib. http://matplotlib.org/.

[18] python-refprop. https://github.com/AndySchroder/python-refprop.

[19] Andy Schroder. Supercritical Carbon Dioxide Power Cycles. http://andyschroder.com/CO2Cycle/.

[20] Ian Bell. CoolProp: Fluid properties for the masses. http://coolprop.sourceforge.net/.